PERGAMON

Vision Research 38 (1998) 3555–3568

Vision Research

Detection and recognition of radial frequency patterns [1]

Frances Wilkinson [a,*], Hugh R Wilson [b], Claudine Habak [a]

[a] *Department of Psychology, McGill University, 1205 Dr. Penfield, Montreal, Quebec H3A 1B1, Canada*
[b] *Visual Sciences Center, University of Chicago, 939 East 57th St., Chicago, IL 60637, USA*

Received 4 September 1997; received in revised form 29 December 1997

Abstract

Detection thresholds for radial deformations of circular contours were measured using a range of radii and contour peak spatial frequencies. For radial frequencies above two cycles, thresholds were found to be a constant fraction of the mean radius across a four-octave range of pattern radii and peak spatial frequencies (mean Weber fraction: 0.003–0.004). At low radial frequencies, thresholds were unaffected by contrast reduction. In 167 ms presentations, subjects were able to identify radial frequencies of six cycles and below with an accuracy of over 90% correct even when phase was randomized. The extreme sensitivity of subjects to these radial deformations (as low as 2–4 s of arc) cannot be explained by local orientation or curvature analysis, and points instead to the global pooling of contour information at intermediate levels of form vision. © 1998 Elsevier Science Ltd. All rights reserved.

Keywords: Circular; Global; Curvature; Shape recognition; Hyperacuity

1. Introduction

Over the past two decades, our understanding of the visual processing of retinal images has made enormous progress at two levels. There is now substantial evidence, based on both psychophysical and electrophysiological data, that the information processing carried out by the early stages of the visual pathway can be modeled by filtering the image through a bank of local linear filters tuned for orientation, spatial and temporal frequency [1–3]. While several synaptic steps are involved in this transformation, the linear model nevertheless provides quite an accurate description of the relationship between the retinal input and the activity of cortical simple cells. At the other end of the scale, single unit electrophysiology in alert primates indicates that neurons at the highest levels of the 'ventral processing stream' [4] in the inferotemporal cortex exhibit considerable response specificity, showing tuning for highly complex patterns such as faces [5–7].

What remains elusive are the transformations which occur between these two levels. An important first step has been the recognition of the critical role played by non-linear (non-Fourier) processing after the simple cell stage. Information that is clearly detectable by human observers in complex visual images is lost in models unless the early linear stage is followed by some form of rectification, which permits us to retain evidence of local changes when information is grouped over a larger region, as in texture perception [8–12]. While this has taken us some distance in understanding visual texture and motion, the same concept has only recently been applied to the study of object shape or form [13,14].

Secondly, we lack a metric for shapes, a notion of what might form a basis set for the meaningful analysis of real world objects, although some important suggestions have been made [15]. One presumes that the development of neural structures in the ventral pathway was guided by evolutionary pressures, and thus evolved to handle in an efficient manner the spatial properties of biologically important natural objects. One of the most striking properties of most natural objects—animals, flowers, clouds etc.—is curvature. Thus a critical question becomes: how do we move from local oriented components—the optimal stimuli for the early filtering process—to the analysis of smoothly curved shapes?

* Corresponding author. Fax: +1 514 3984896; e-mail: fran@hebb.psych.mcgill.ca.

[1] This research was first reported at the annual meeting of the Association for Research in Vision and Ophthamology, 1996.

PII: S0042-6989(98)00039-X

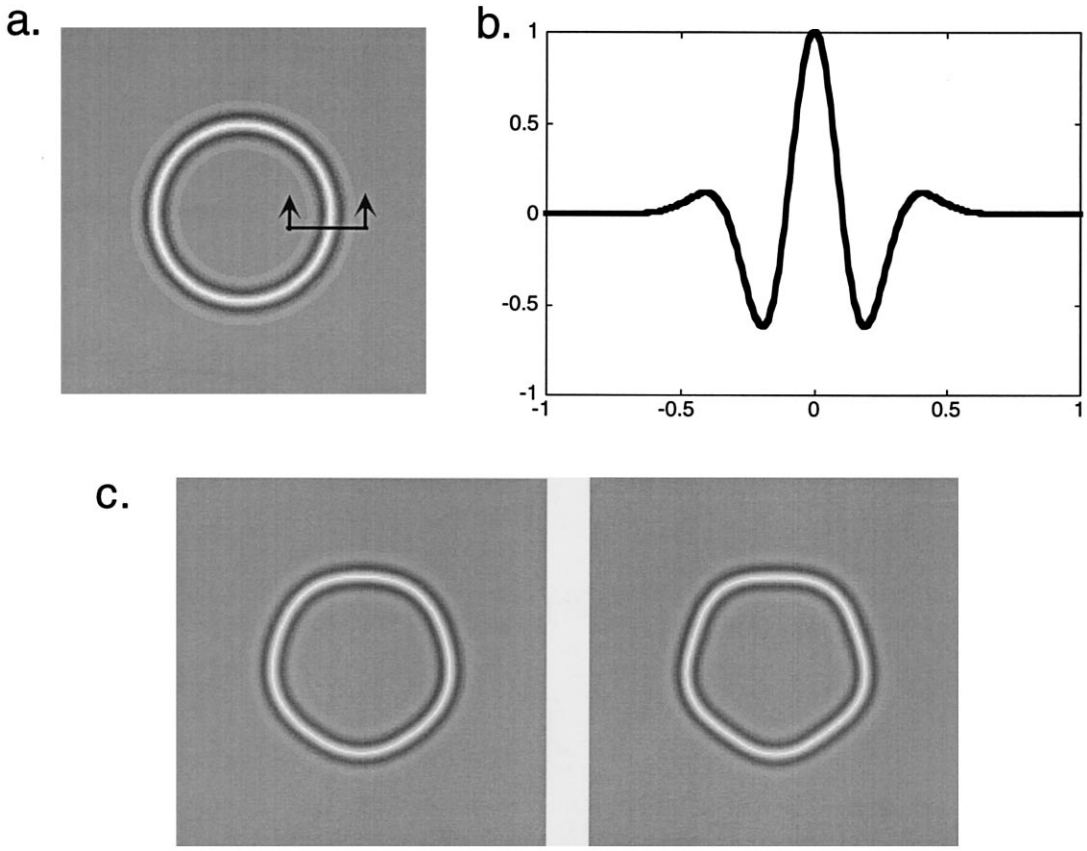

Fig. 1. (a.) Example of the D4 circles used as stimuli in this study. If viewed at a distance such that the radius of the circle subtends 0.5°, the peak spatial frequency of this circle will be 8 cpd. (b.) Cross-sectional luminance profile of the D4 contour as indicated by the arrows in (a). (c.) Examples of patterns with radial frequencies of five cycles. The peak amplitudes (A in Eq. (3)) are 0.015 and 0.03 for the left and right patterns respectively.

Our object in this paper is to explore perception of curved shapes using a novel stimulus set based on deformations of circles. As these patterns are defined by sinusoidal modulation of the radius in polar coordinates, we term them radial frequency (RF) patterns A major impetus for this study has been the recent electrophysiological work of Gallant et al. [16,17], showing that a subset of neurons in primate V4 are optimally tuned to non-Cartesian stimuli-concentric and hyperbolic forms. Stimulated by these findings, we have previously provided evidence that the human visual system is capable of global, concentric orientation summation in the detection of random dot Glass [18] patterns. These data were shown to be consistent with a non-Fourier model in which the outputs of simple cell filters were combined in a biologically plausible fashion to produce units optimally tuned for quasi-circular patterns [13]. Furthermore, responses of this model are in good agreement with the non-Cartesian V4 units of Gallant et al. [16,17]. In the present study, we examine psychophysically the sensitivity of normal human observers to small deviations from circularity. The thresholds we report, which are hyperacuities over a large range of our stimulus set, provide further evidence that the human visual system has special sensitivity for this class of pattern. Further experiments indicate that a subset of these radial frequency patterns can be recognized almost perfectly in 167 ms presentations. Our results cannot be explained by local contour processing but instead require some form of global analysis such as that reported by Wilson et al. [13].

2. Methods

2.1. Stimuli

2.1.1. Base circles

The base pattern used in this study is a circular contour with a cross-sectional luminance profile defined by a radial fourth derivative of a Gaussian (D4) (see Fig. 1a and b). The equation for the circles is:

$$\mathrm{D4}(r) = C\left(1 - 4\left(\frac{r - r_0}{\sigma}\right)^2 + \frac{4}{3}\left(\frac{r - r_0}{\sigma}\right)^4\right) \times \exp\left(-\left(\frac{r - r_0}{\sigma}\right)^2\right) \quad (1)$$

where r_0 is the mean radius, C is the pattern contrast, and σ determines the peak spatial frequency (see Eq. (2)). Provided $r_0 > 4\sigma$, the radial D4 integrates very nearly to zero across its width, resulting in a pattern that is band limited in spatial frequency. The peak spatial frequency of a D4 is:

$$f_{\text{peak}} = \frac{\sqrt{2}}{\pi\sigma} \tag{2}$$

and its full spatial frequency band-width is 1.24 octaves at half amplitude.

2.1.2. Radial frequency patterns

The base circles are deformed by applying a radial sinusoidal modulation to the radius r_0 in Eq. (1) such that the radius of the deformed pattern at polar angle θ in radians is:

$$r(\theta) = r_0(1 + A \ \sin(\omega\theta + \phi)) \tag{3}$$

where r_0 is the mean radius, A is the radial modulation amplitude, and ω is the radial frequency. The angular phase of the pattern is determined by ϕ. These patterns differ significantly from the Fourier descriptors which were introduced to physiological studies by Schwartz et al. [19], a point to be elaborated in Section 6. For consistency, we shall always refer to f_{peak} in Eq. (2) as the spatial frequency, ω in Eq. (3) as the radial frequency, and A in Eq. (3) as the radial amplitude.

Two restrictions are placed on the parameter values in Eq. (3). Radial amplitude (A) is not permitted to exceed 1.0 and radial frequency (ω) is always an integer value. This gives rise to patterns of defined numbers of lobes bounded by a D4 contour which is closed and never crosses itself, both characteristics of object boundaries. In Fig. 1c, radial amplitudes of 1.5 and 3% are shown for a radial frequency of five cycles. Fig. 2 shows the complete set of radial frequencies used in this study, in each case well above threshold. Radial amplitude (A in Eq. (3)) is the amplitude of the sinusoidal modulation expressed as a proportion of the radius.

Stimuli were generated on a Macintosh IIvx computer with a 67 Hz frame rate. Contrast linearization was implemented with 150 equally spaced gray levels. Screen resolution was 640×480 pixels, and pattern luminance was modulated about a mean of 70 cd/m^2. D4 contrast was 100% except where otherwise indicated. The other parameters of the RF patterns will be described separately for each experiment. Subjects viewed the stimuli under dim room illumination at a usual viewing distance of 187 cm. At this distance, the screen subtended a visual angle of $6.4 \times 4.8°$. For some of the extreme radii and peak spatial frequencies tested in Experiment 1 it was necessary to alter the viewing distance as well as the screen parameters of the stimuli in order to achieve the desired angular stimulus values.

We report below the results for three sets of experiments based on this stimulus set. In Experiment 1, basic detection thresholds are assessed for a range of radial frequencies, radii, and spatial frequencies, and a number of control conditions are examined in an effort to determine the critical cue underlying these thresholds. In Experiment 2, the dependence of the thresholds on image contrast is examined, and performance is compared to a second task based on sinusoidal modulation of straight lines. Finally, in Experiment 3, the ability of subjects to identify patterns on the basis of their radial frequency is examined.

3. Experiment 1: basic thresholds

3.1. Procedure

The ability of subjects to detect deformations of the base circles was examined using a two-alternative temporal forced choice paradigm and the method of constant stimuli. Within an experimental run, circle radius, spatial frequency and radial frequency were held constant, and the radial amplitude was varied randomly on a logarithmic scale. The comparison stimulus was always the matching base circle. No fixation point was

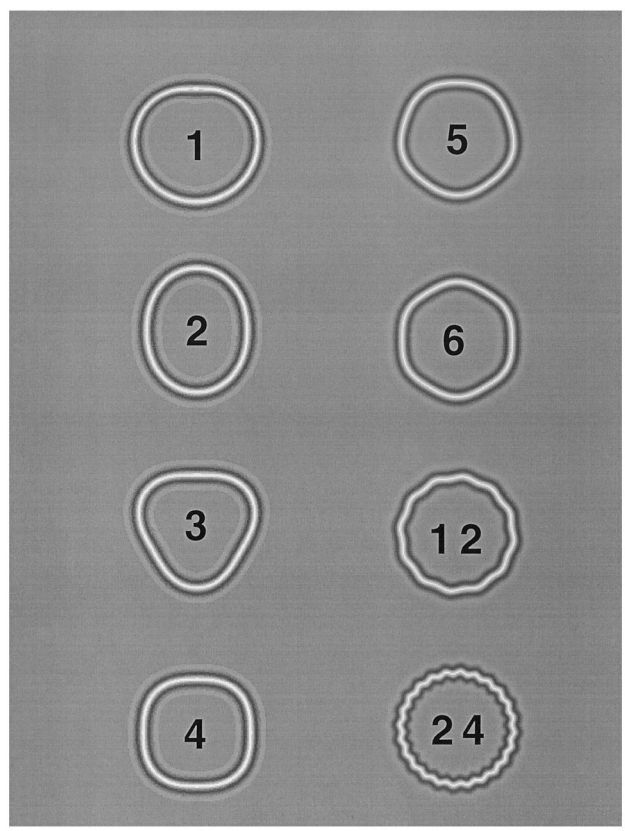

Fig. 2. Examples of the radial frequencies used as stimuli in Experiment 1. The amplitudes of the patterns illustrated are five to ten times greater than threshold.

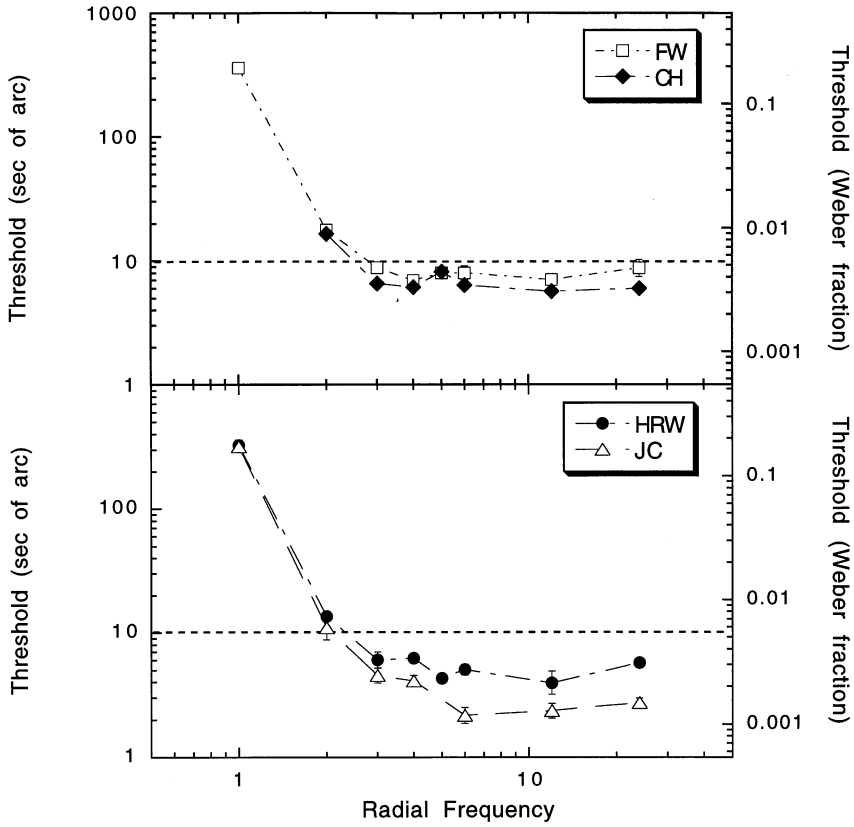

Fig. 3. Modulation detection thresholds for four subjects for radial frequency patterns ranging from 1 to 24 cycles. Thresholds (minimum modulation amplitude) are expressed in visual angle on the left ordinate and as proportions of the radius of the base circle (Weber fraction) on the right ordinate. Subject JC (lower panel) was tested binocularly; all other subjects were tested monocularly with their preferred eye. Error bars = 1 S.E.

used. Subjects were instructed to fixate the center of the screen and to indicate in which of two 500 ms intervals the deformed pattern appeared by pressing one or two on the computer keyboard. Except where otherwise specified testing was monocular, with subjects using their preferred eye. Feedback was not provided.

Stimuli were offset from the center of the computer screen by a small random spatial jitter, which at its maximum equaled $\pm 33\%$ of the circle's radius. This jitter was introduced because one of the radial frequencies (RF1) introduces a translation as well as a distortion of the patterns, and we wished to eliminate translation as a cue. Control tests indicated that thresholds were not degraded by the addition of this small spatial jitter at any radial frequency.

For each set of base circle parameters examined (radius and spatial frequency), thresholds were evaluated for several radial frequencies. The order of radial frequencies tested was randomized across runs.

3.2. Subjects

The three authors and four naive observers participated in Experiment 1. All subjects had corrected to normal visual acuity.

3.3. Results

3.3.1. 8 cpd 0.5° radius

In the first phase of this study, thresholds were measured for radial frequencies ranging from 1 to 24 cycles (see Fig. 2). The base circle had a peak spatial frequency of 8 cpd and a radius of 0.5°. The results for four subjects are displayed in Fig. 3. Three of the subjects were tested monocularly, and the fourth (JC) was tested binocularly. All four subjects showed a very similar pattern of results. Thresholds fell almost 2 log units from a high at RF1 to an asymptotic value which was reached between RF3 and RF5 in different subjects. When the amplitude of the minimum detectable distortion is expressed in s of arc (left ordinate), it is clear that these values fall well within the 'hyperacuity' range for radial frequencies above RF2, with asymptotic values ranging from 2–9 s of arc. Expressed as a proportion of the radius (Weber fraction-right ordinate), the asymptotic values averaged 0.003. It is important to note that the thresholds for RF3 and 5 are very similar to those for RF4 and 6. Since the diameters of odd-numbered patterns do not vary at any point around the deformed patterns, the constant Weber fractions must be referred to the radius and not the diameter.

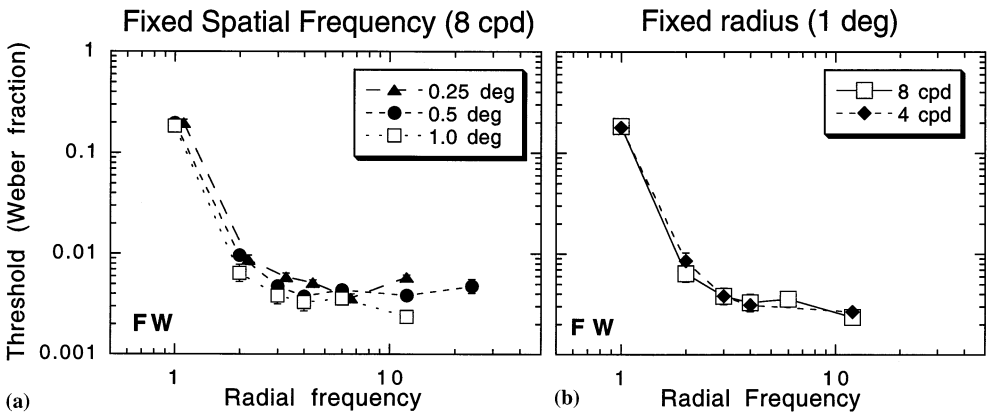

Fig. 4. (a) Modulation detection thresholds for one subject for patterns of fixed peak spatial frequency (8 cpd) and radii of 0.25, 0.5 and 1.0° plotted against radial frequency. (b) Modulation detection thresholds for the same subject tested with RF patterns of 1° radius and peak spatial frequencies of 4 and 8 cpd. Error bars = 1 S.E.

3.3.2. Scaling of radius and spatial frequency

In order to determine the dependence of these thresholds on the spatial frequency and the radius of the patterns, we varied these parameters independently across a range of radial frequencies. We initially examined three radii (0.25, 0.50 and 1°) and three spatial frequencies (4, 8 and 16 cpd). When D4 peak spatial frequency was held fixed at 8 cpd (the original test spatial frequency), varying the pattern radius by a factor of four had little effect on the thresholds expressed as Weber fractions. As illustrated in Fig. 4(a) for subject FW, the threshold curves for the three radii very nearly superimpose. A second subject (not shown) tested at radial frequencies 2, 3 and 4 showed a similar superposition. Since the Weber fractions are very similar, the angular values of the thresholds at each radial frequency increase with radius. Nevertheless, it is interesting to note that thresholds for radial frequencies above two cycles never exceeded 25 s of arc, even for a 1.0° diameter circle, indicating sensitivity to displacements of less than the diameter of a foveal cone.

Fig. 4(b) illustrates the converse situation in which circle radius was fixed at 1°, and the spatial frequency of the D4 contour was varied by an octave. Again the curves superimpose completely, indicating that, at least over this limited range, contour spatial frequency does not affect sensitivity to deformations at any radial frequency.

In the natural world, spatial frequency and radius vary inversely as viewing distance is altered. We next simulated the effects of changing viewing distance by measuring thresholds over a range of three radii (0.25–1°), at the same time varying spatial frequency over a corresponding two octave range (16–4 cpd). The results of this comparison are presented in Fig. 5 for three subjects. It is clear that thresholds for the larger two pattern sets (circles and squares in Fig. 5 are very similar at each radial frequency indicating excellent distance scaling. There is some fall-off in performance for the smallest pattern set (0.25° radius, 16 cpd) which is apparent in all subjects at the higher RFs, and is evident in FW at all RFs above two cycles. This is presumably a consequence of using a spatial frequency within 1–1.5 octaves of the resolution limit of our subjects. Again, it must be noted that in angular terms, these apparently elevated thresholds for the small high spatial frequency circles still fall under 15 s of arc.

To summarize the findings in Fig. 4 and Fig. 5, over a two octave range of radii and spatial frequencies, radial frequency patterns maintain shape constancy at threshold. In other words, the proportions of an RF pattern at the point at which it becomes distinguishable from a perfect circle are identical, as indicated by the Weber fraction thresholds. We were interested in exploring this issue more fully by extending our testing to a greater range of radii and spatial frequencies. To do so, we limited our examination to a single radial frequency (RF5) which was not extensively tested in the above manipulations, and tested one experienced observer (CH) and one naive observer (JG) on a range of stimulus conditions combining spatial frequencies from 1 to 16 cpd with radii of 0.25–4.0°. It should be noted that not all combinations from these ranges are possible—for any radius there is a spatial frequency limit below which the two inner edges of the D4 contour will overlap. To avoid this situation we only tested cases in which the radius was equal to or greater than 1/peak spatial frequency.

The results of this testing are displayed in Fig. 6. Both subjects showed the same general pattern of results. Weber fraction thresholds were very similar across the entire test range with the exception of the smallest, highest spatial frequency pattern (0.25° radius, 16 cpd). The mean thresholds, excluding this point, were 0.0042 and 0.0044 for CH and JG respectively (range 0.0030–0.0054), whereas the thresholds for the

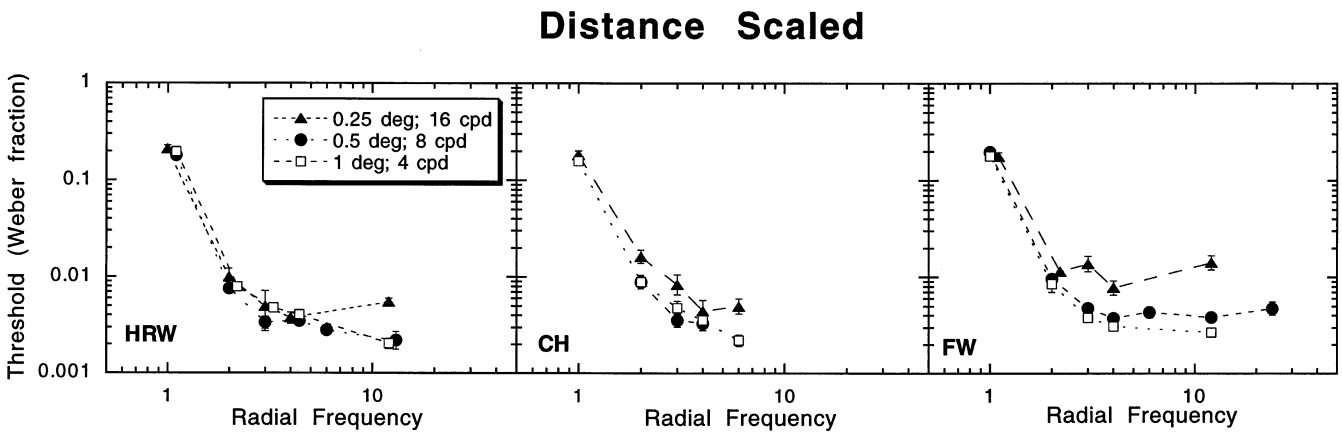

Fig. 5. Modulation detection thresholds for three subjects tested with stimuli in which radius (0.25–1.0°) and peak spatial frequency (4–16 cpd) were scaled inversely. In each case thresholds (proportion of the radius) are plotted against radial frequency. Error bars = 1 S.E.

smallest pattern were approximately double these values (0.0076 and 0.0087, respectively). This confirms the finding described above that performance begins to drop off for small, high frequency patterns or, stated differently, the shapes must be more exaggerated before they are perceived as differing from circles. However, over most of a 4 octave range of spatial frequencies and radii, performance remains nearly constant. This is true despite the fact that in the most extreme cases tested, the contours lie 4° away from the foveal centre.

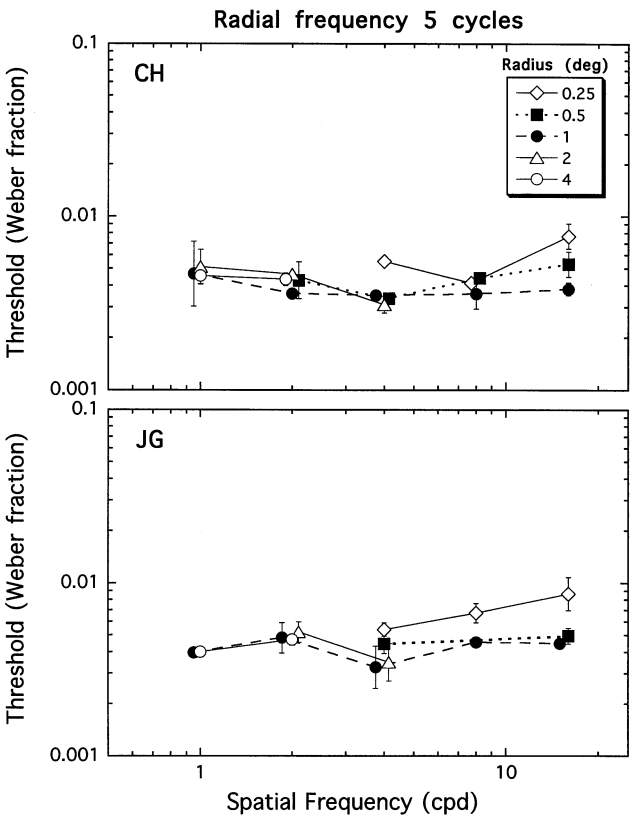

Fig. 6. Modulation detection thresholds for two subjects (CH and JG) tested with RF5 patterns radii 0.25–4.0° plotted against peak spatial frequency. Error bars = 1 S.E.

3.3.3. Control experiments: radius

The thresholds we have reported above were described as Weber fractions or proportions of the radius of the base circle. However, this does not imply that difference in radius is the cue used by subjects to perform this discrimination. To address this issue, the following control experiment was conducted.

If detecting differences in the maximum (or minimum) radius between the deformed test stimuli and the comparison circles were the critical variable, subjects should be able to discriminate between two perfect circles of differing radii with as great sensitivity. To test this, two subjects (HRW and a naive subject DE) were tested on a two alternative temporal interval discrimination between a 0.5° radius, 8 cpd D4 circle and D4 circles of increasing radii. They were instructed to choose the larger circle in each case. The Weber fraction for circle radius discrimination averaged 0.025 compared to a Weber fraction on average of 0.003 for discriminating radial frequencies 3–24 cycles, approximately an eight-fold difference in threshold.

3.3.4. Control experiments: curvature

As the radius changes, either locally in the radial frequency patterns, or globally as the base circles are enlarged, local curvature of the contour describing the circle is also changing. It is therefore possible that the discrimination is based on local contour curvature, since a radial frequency pattern has both higher and lower curvature than the comparison circle. Curvature difference could therefore provide a cue to differentiating the RF patterns from the base circle. The curvature of a circle is constant and inversely proportional to the radius of the circle, and therefore may be easily calculated. The local curvature of radial frequency patterns varies around their perimeter, but a more complex calculation shows that the maximum curvature K is given by:

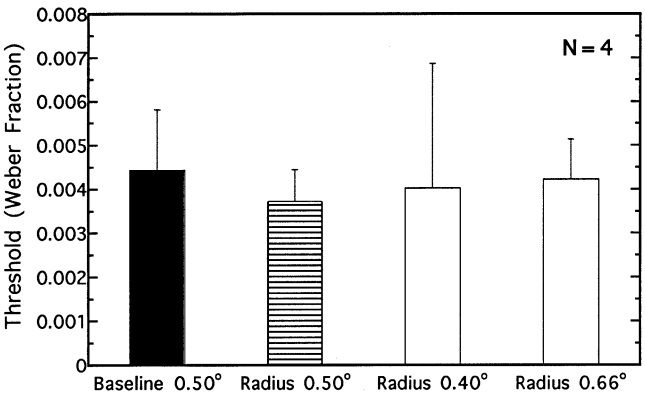

Fig. 7. Average modulation thresholds for four subjects. In all conditions, radial frequency was five cycles. In the baseline condition (black fill) RF5 patterns of 0.5° mean radius were discriminated from circles of equal radius. In the critical test condition (horizontal fill), RF5 patterns of 0.50° mean radius were discriminated from circles of radii 0.40–0.66°. In the two remaining conditions (white fill), RF5 patterns of 0.40 and 0.66° mean radii were discriminated from circles of radii 0.40–0.66°. Error bars = S.D.

$$\kappa = \frac{A\ \omega^2 + A + 1}{R_0(1+A)^2} \tag{4}$$

where A is the radial amplitude, ω is the radial frequency and R_0 is the mean radius. Thus maximum curvature is dependent both on the amplitude of the radial modulation, and on the square of the radial frequency. Minimum curvature is obtained by replacing A with $-A$ in this formula.

Using Eq. (4), we calculated the maximum and minimum curvature for 0.5° radius RF5 patterns of amplitude 0.01. This is about three times the threshold amplitude, and represents one of the largest amplitude stimuli used in measuring psychometric functions. We then determined the radii of circles of curvature equal to these maximum and minimum values: the critical radii were found to be 0.40 and 0.66°, respectively.

We reasoned that by pairing the RF5 patterns (radius 0.50°) with circles of 0.40, 0.50 and 0.66° radius at random, local curvature would no longer provide a reliable cue. In order to eliminate pattern radius (or overall size) as a cue, we simultaneously measured thresholds for RF5 patterns of 0.40 and 0.66° base radii, again paired at random with the three base circles. Thus, within a run in this experiment, the radii of the test (RF5) and comparison (circle) stimuli varied independently from trial to trial.

We tested four subjects on this task, two of the authors (HRW and FW) who had participated extensively in the earlier parts of the study and two naive observers (RD and MC) with limited experience with radial frequency patterns. The results are presented in Fig. 7. The black bar represents baseline RF5 thresholds from the condition described in Experiment 1. The critical test condition is the threshold measured for the same RF5 pattern (radius 0.5°) when the radius of the comparison circle varied randomly from 0.40–0.66°. The second (cross-hatched) bar represents the results for this condition. It is very clear that this manipulation did not lead to an elevation in threshold, as would have been predicted if the subjects were using local curvature as the critical cue. In fact, two of the four subjects showed slight reductions in threshold in this condition, and a third showed no change. The remaining two bars in the histogram indicate that performance with the smaller or larger RF5 patterns was not disrupted by testing with the three comparison stimuli, although there was greater variability across subjects with the smaller RF5 patterns (radius 0.40°).

4. Experiment 2: comparisons to sinusoidally modulated straight line

Hyperacuities have been reported in many other detection tasks over the years [20]. Most relevant in the current context is the work of Tyler [21] on detection of sinusoidal modulation of straight lines. If detection of such modulation in both lines and circles reflected thresholds for detecting local change in the contour (e.g. orientation, curvature), one might expect to see comparable performance on these two tasks under a variety of parametric manipulations. To examine this issue, we have devised a band-limited variant of the Tyler stimulus, and have compared performance on this task to thresholds for radial frequency patterns over a range of contrasts.

4.1. Stimuli

The base stimulus is two straight contours with the same D4 luminance profile as the circles described previously (Fig. 8). The length of each line is one half the circumference of the base circular pattern, which

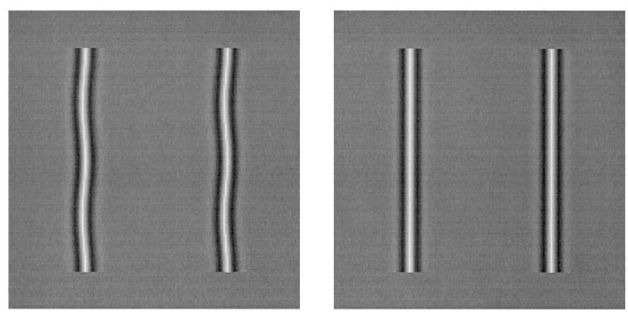

Fig. 8. Sinusoidally modulated line pair (left) and comparison pair of unmodulated lines (right). Luminance profile of the lines is the defined by the fourth spatial derivative of a Gaussian (D4) as in Fig. 1b. Total modulation = four cycles; two cycles per line. Performance on this discrimination was compared to performance discriminating RF4 patterns (see Fig. 2) from circles. Inter-line spacing was equated to the diameter of the circle in the RF4/circle discrimination, and total line length to the circle circumference.

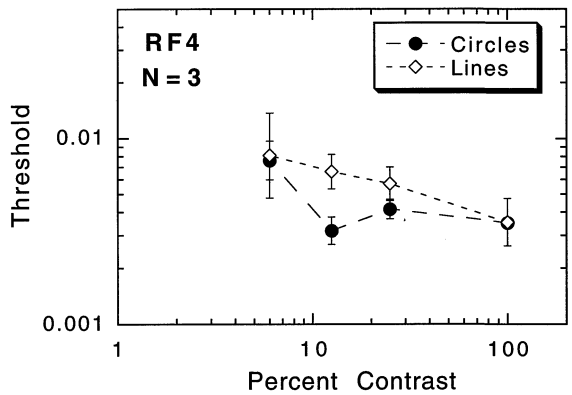

Fig. 9. Threshold performance averaged for three subjects for detecting four cycles of sinusoidal modulation of circles (filled circles) and lines (open diamonds) plotted against pattern contrast. Error bars = 1 S.D.

equates total contour length. Line separation is equal to the circle's diameter. Thus the lines occur at roughly the same retinal eccentricity as the circles to which they are being compared. Sinusoidal modulation of the same total number of cycles is then applied to the lines. For both lines and circles, modulation amplitude is expressed as a proportion of the circle's radius (or of half the distance between the lines).

4.2. Procedure

Thresholds for detecting four cycles of modulation in line and circle patterns were measured in the three authors (FW, HRW, CH). Within an experimental run, pattern type and contrast remained fixed. Four contrast levels were tested (100, 25, 12.5 and 6.25%). Because of slope differences found between the circle and line conditions, we extended our measurements to sinusoidal modulation frequencies of 2, 3, 6, and 12 cycles (over the line pair) at 100 and 12.5% contrast in two subjects (FW and CH), and to five cycles in subject FW.

4.3. Results

The mean performance of subjects on line and circle patterns of four cycles modulation frequency is compared in Fig. 9. At 100% contrast, thresholds on the two tasks are very similar (Weber fraction $= 0.0035$). However, for the line stimuli, the relationship between thresholds and contrast was found to be a power function with exponent of 0.29, whereas thresholds for the circles showed no decline down to 12.5% contrast. Only at the lowest contrast tested (6.25%) did performance fall off to the same level as seen for the line patterns.

To see whether this difference in contrast performance affected the full range of modulation frequencies, we measured thresholds at 100 and 12.5% contrast for several additional frequencies. The exponents of the power functions joining these two points for each modulation frequency are listed in Table 1(A). Two points are clear from inspecting the data. Firstly, for every radial frequency tested for each subject, the exponent was lower for the circle stimuli than for the line stimuli. These differences were tested statistically for FW and CH separately using the Wilcoxon matched-pair signed rank test and were found to be significant ($P = 0.028$ and $P = 0.043$, respectively). HRW showed the same pattern of results for the single condition tested (RF4). This provides a clear indication that the processes underlying the detection of modulations of lines and circles are not the same.

The second point apparent in the data is that for low radial frequencies there is evidence of a strong contrast gain control operating. As can be seen in Table 1(B), the mean exponent for all data sets collected for RF2–4 circular patterns was very close to zero, indicating that performance was unaffected by contrast reduction from 100 to 12%. Above four cycles, the functions had clear negative slopes, although the exponents remained lower than those for the comparable line stimuli.

5. Experiment 3: radial frequency identification

If the mechanisms underlying the sensitivity to radial frequency patterns reported above actually play a role in shape and object recognition, one would expect subjects to be able to discriminate among patterns of differing radial frequencies. We have examined this issue by asking subjects to identify briefly presented

Table 1
(A) Exponents of the power functions relating modulation detection thresholds to pattern contrast for a range of modulation frequencies; (B) mean exponents averaged over subjects and over the modulation frequencies indicated

Mod. Freq.	Subject	Circles	Lines
A			
2	FW	−0.04	−0.20
	CH	0.02	−0.39
3	FW	−0.04	−0.18
	CH	−0.11	−0.62
4	FW	−0.04	−0.40
	CH	0.04	−0.17
	HRW	0.11	−0.37
5	FW	−0.31	−0.43
6	FW	−0.16	−0.34
	CH	−0.20	−0.28
12	FW	−0.34	−0.49
	CH	−0.39	−0.45
B			
2–4		−0.01	−0.33
5–12		−0.28	−0.40

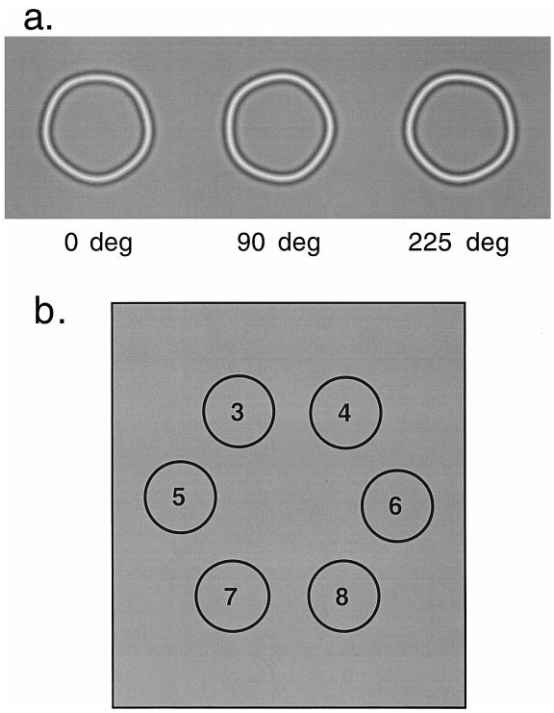

Fig. 10. (a.) RF5 patterns of three phase angles used in the RF identification task. (b.) Identification template. Subjects indicated the number of lobes in the stimulus pattern by moving the computer cursor into the appropriately numbered circle. In the second condition (RF5–10) numbers in the template ranged from 5 to 10 in the same ascending spatial pattern.

exemplars of six radial frequency patterns, in the first instance ranging from three to eight cycles, and in the second instance, from five to ten cycles.

5.1. Stimuli and procedure

The stimuli all had mean radii of 0.5°, spatial frequencies of 8 cpd, and radial amplitudes of approximately three times the mean thresholds measured in subjects in Experiment 1 for stimuli of identical spatial parameters. RF patterns can be rotated about their centers by varying the phase of the sinusoidal modulation of the base circle's radius (ϕ in Eq. (3)). For each radial frequency, three phase angles were used (see Fig. 10(a) for example). On each trial, a single RF pattern was presented for a brief exposure (167 ms) followed by a template showing six circles each containing a digit (Fig. 10b). Subjects were instructed to use the computer mouse to move the cursor onto the circle corresponding to the number of lobes in the shape they had just seen. We used digits to represent the shapes rather than actual templates because multiple phases or rotations of each shape were presented, and we wanted to determine whether our subjects could generalize across these variants.

Subjects for this study included a total of ten observers, five experienced with these patterns from their participation in earlier parts of the study, and five naive observers. Each subject was tested on both the lower (RF3–8) and higher (RF5–10) variants of the task. Within a task, each radial frequency was presented 75 times, with both order of RFs and pattern phase randomized. In addition, position was randomized by $\pm$ 33% of the radius as in the previous studies. Task order (lower vs higher RF set) was counterbalanced across subjects. We examined both the percentage of correct identifications of each RF pattern, and the pattern of errors made by subjects.

5.2. Results

The results are illustrated in Fig. 11. Regardless of the range of frequencies tested, median performance was above 90% correct for radial frequencies 3–6 inclusive, and then fell off dramatically. The slight increase in performance for the highest frequency in each condition is presumably due to a tendency to guess the maximum RF when there appears to be many sides. The lower panel indicates the number of times a radial frequency value was erroneously assigned to a pattern of higher or lower RF (false alarms). The error data show a mirror image of the recognition scores. Subjects rarely misidentified the lower frequency patterns; however, frequencies of six cycles and higher were frequently chosen in error, usually as responses to other high frequency patterns. Thus although observers are equally sensitive in detecting low and high frequency

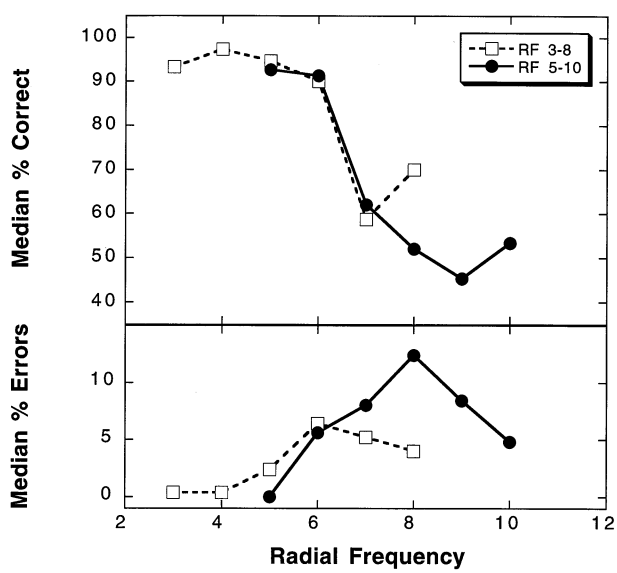

Fig. 11. Upper panel. Identification performance (median % correct) for ten subjects plotted against radial frequency in conditions with RF patterns ranging from three to eight cycles (open squares) and from five to ten cycles (filled circles). Lower panel. Corresponding false alarm rate (% errors) plotted against radial frequency for the same two conditions. The false alarm rate is the percentage of trials on which a pattern was incorrectly identified as being of each radial frequency (of a possible 125 trials).

modulations of a circle (Fig. 3), there is none the less a clear difference in the ability of the recognition system to handle few-sided and many-sided pattern.

6. Discussion

The principal finding of this study is that humans are exquisitely sensitive in detecting and recognizing small deviations from the circular form. The novel class of radial frequency patterns used here has allowed us to demonstrate two important points about this sensitivity. First, for a given radius sensitivity is equivalent for radial frequencies spanning at least the range from 3–24 cycles of sinusoidal modulation, although thresholds do fall off markedly for frequencies below three cycles. Secondly, thresholds expressed as a proportion of the radius (Weber fractions) are constant across a 4-octave range of radii and contour spatial frequencies. The consequence of this point is that a pattern of a given radial frequency always has the same shape at its threshold amplitude, independent of its size or spatial frequency content.

Although our radial frequency patterns are novel to psychophysical experimentation, there are several previous studies related to ours. Both Laursen and Rasmussen [22] and Regan and Hamstra [23] measured thresholds for discriminating a circle from an ellipse and obtained average Weber fractions of 0.0125 and 0.011, respectively. In the former study, psychophysical thresholds for humans and monkeys were found to be similar. Near threshold our RF2 pattern is a very close approximation to an ellipse, and our mean Weber fraction of 0.0085 is in reasonable agreement with these previous studies. Our data for RF patterns show that deformation of a circle into an ellipse produces significantly higher thresholds than deformation of a circle into an RF3 or higher pattern. Furthermore, the lower thresholds for radial frequencies greater than two cast doubt on the model suggested by Regan and Hamstra [23], which involved the ratio of two neural pools: one determining vertical extent, and one determining horizontal extent. Such a scheme would fail for radial frequencies 4, 6, 8, etc., as the horizontal:vertical aspect ratio remains 1:1. Despite this, our study agrees with Regan and Hamstra [23] in concluding that global rather than local processing (see below) must be involved in determining both RF and ellipsoidal thresholds.

In a shape similarity study, Shepard and Cermak [24] used stimuli defined by periodic variation of the radius in polar coordinates. While these patterns are related to our RF patterns, the Shepard and Cermak [24] patterns employed exponential functions with periodic exponents. By summing six such components to define their radii, these authors were able to generate smoothly curved stimuli that were reminiscent of natural organic shapes. Interestingly, they reported evidence that their period two and three patterns, analogs of our RF2 and RF3 patterns, were perceptually independent. This is consistent with our recognition experiments in which radial frequencies of six or less could be identified almost perfectly during 167 ms exposures.

The falloff in identification performance for radial frequencies above RF6 is striking. One possible explanation is that it may represent another instance of what has been termed subitizing [25] in numerosity judgments. It has long been known that human observers are able to indicate accurately the number of dots in a random array up to a limit of between five and eight [26,27]; beyond this number, performance is degraded unless the elements can be organized into distinct groupings. Indeed many aspects of human information processing show a similar limitation, a phenomenon Miller labeled 'the magical number seven plus or minus two' [28]. Alternatively, we suggest below that this result may reflect the 'resolution' limit of the neural mechanism encoding the global structure of our patterns.

6.1. Critical factors underlying discrimination

6.1.1. Local cues

The observation that over a wide range, the thresholds we have measured follow Weber's Law with respect to the circle radius implies that the measure being used by the visual system is either the radius of the patterns or some other parameter which varies as a function of the radius. We have shown in a control experiment that subjects cannot assess the radius itself to the necessary level of accuracy; in fact thresholds were eight times higher for discrimination between two perfect circles than between a circle and an RF pattern of at least three cycles.

Which other simple measures vary with the radius and yet permit local assessment of the changes which differentiate an RF pattern at threshold from a perfect circle? The two obvious possibilities which must be considered are local contour orientation and curvature. Let us first consider orientation. When an RF pattern is compared to a circle of equal mean radius, the maximum difference in local orientation of the contours of the circle and of the RF pattern occurs where the RF pattern is in sine phase (see Fig. 12(a) black arrows). This orientation difference remains constant as the radius of the circle/RF pair is varied. However, two factors allow us to rule out local orientation difference as the critical cue in this discrimination task. Firstly, in our paradigm, the position of the stimuli was jittered by up to $\pm 33\%$ of the radius in both X and Y dimensions. This would make it impossible to compare the same point on the two patterns, without first referencing the

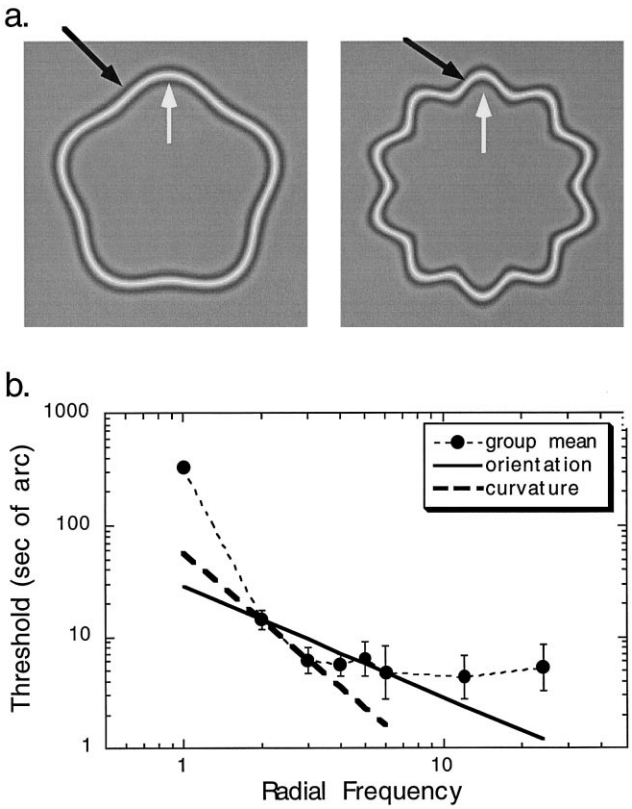

Fig. 12. (a.) Radial frequency patterns of five (left) and ten (right) cycles of sinusoidal modulation of equal amplitude (0.08). The black arrows indicate the points of maximum orientation difference from a circle of equal radius centered at the same point. The white arrows indicate the points of maximum curvature difference. (b.) Average detection thresholds for four subjects (individual data in Fig. 3) plotted against radial frequency. The solid and dashed lines represent the predicted performance for discrimination based on local orientation and curvature respectively. Both sets of predictions have been based on average performance for RF2, the point at which the best fit to the data is obtained.

point to the centers of the patterns, which by definition would require a global measure. Secondly, the maximum orientation change at a particular radial amplitude increases linearly with radial frequency (Fig. 12 a and b). The implication of this is that if the threshold for our discrimination were set by the maximum orientation difference between a circle and an RF pattern, thresholds should decrease with a slope of -1.0 with increasing radial frequency. As shown in Fig. 12b, this provides a very poor fit to our data.

It is interesting to note that local orientation comparison is the explanation put forward by Tyler [21] to explain the hyperacuity thresholds he obtained for his sinusoidal line stimuli. In Tyler's case, there was a single vertical standard which was presented as the comparison stimulus and which could presumably also be generated internally by the subject. Thus, the task could be performed by determining whether any local orientation in the stimulus differed significantly from vertical. However, in the present case, since a circle contains all orientations, any orientation on the pattern circumference must be referenced to the circle center to determine whether it is an RF pattern, and this would entail global processing of the circle.

Local curvature offers another potential cue for distinguishing between a circle and an RF pattern of equal mean radius. The curvature of a circle is constant around its circumference, whereas the curvature of an RF pattern varies with the periodicity of the radial frequency. Thus an RF pattern will have points of both greater and lesser curvature than its comparison circle. Therefore, in principle, one could perform the discrimination by choosing the pattern with either the maximum local curvature or the minimum curvature. However, two findings of the present study make this an untenable explanation. First, in a control experiment circles and RF patterns of varying radii were randomly paired in such a way that in many instances the circle had either the highest or the lowest curvature, but no degradation of performance was seen relative to the case in which the mean radii of both patterns were equal. Secondly, the maximum curvature increases with the square of the radial frequency (see Fig. 12a, white arrows and Eq. (4)) and therefore the slope of the function should be twice as steep as that relating orientation difference to radial frequency. As can be seen in Fig. 12b, this maximum local curvature function provides an even poorer fit to our data with varying radial frequency.

Finally, if local curvature discrimination were the explanation for our results, then discrimination should be easier between circles of varying radius rather than between a circle and an RF pattern. This is because the maximum deviation of RF curvature from that of a circle with the same mean radius only occurs at discrete points (which the subject would somehow have to locate), while two circles of slightly different radius have different curvatures everywhere. As noted above, however, subjects are approximately eight times better at discriminating radial frequency patterns above RF2 than they are at circle radius discrimination. Furthermore, local curvature thresholds using curved segments corresponding to one quarter of a circle have been reported, and these thresholds correspond to a Weber fraction of 0.05 when the base curvature is 2.0 (radius of 0.5°) [29,30]. Thus, local curvature thresholds are over an order of magnitude higher than the Weber fractions of 0.003 that are typical with RF patterns. Watt and Andrews [31] also addressed the issue of local curvature discrimination. Their reported thresholds for a base radius of 0.25° and an arc length equal to a quarter of a circle correspond to a Weber fraction of 0.03. Again it must be concluded that local curvature variation cannot explain our results.

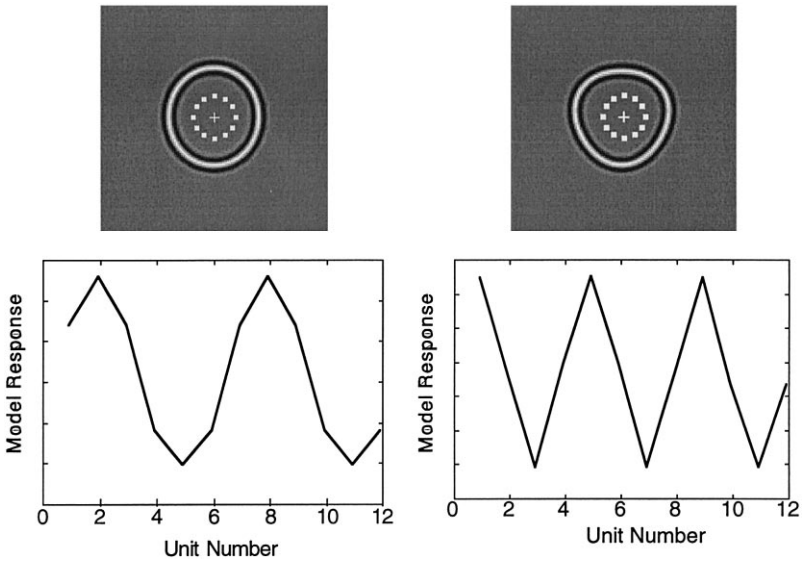

Fig. 13. Responses of simulated V4 concentric unit arrays [13] to RF2 and RF3 patterns (left and right, respectively). The location of the maximally responding unit is plotted by a + in the upper stimulus diagrams. Locations of the 12 neighboring units equidistant from the center unit and from each other are indicated by small squares in the diagrams, and responses of these 12 units are plotted in the lower graphs. It is apparent that this array surrounding the most active unit encodes the radial frequency of the stimulus using population coding.

6.1.2. Global cues

From the above analysis we conclude that the discrimination performed by our subjects cannot be explained locally, using spatial filters which code orientation (e.g. simple cells) or local curvature (e.g. endstopped cells; [32–34]). Instead, a more global analysis is required. This could take one of two forms, which correspond to two basic approaches taken to shape recognition in computer vision [35]. The first is an object-centered approach in which contour information is pooled relative to the center of an object or an object region. The alternative is a sequential, contour-based analysis in which rate of change of some local cue is accumulated sequentially along the contour of the shape. This dichotomy may be illustrated by contrasting our radial frequency stimuli with the Fourier descriptors [36] introduced to biological vision research by Schwartz et al. [19]. As described above, RF patterns have an object-centered definition: they are described by modulation of the radius in polar coordinates (radial frequency, amplitude, polar phase). Fourier descriptors, on the other hand, have a sequential, contour based description. One must first measure contour orientation as a function of contour length along the closed curve, after which Fourier analysis must be applied to this contour orientation function to extract the Fourier descriptors [36]. While local contour orientation is readily extracted by V1 simple cells, there is no evidence for any neural mechanism that can compute the length of arbitrary curved contours. On the other hand, simple neural networks for extracting radial frequencies can be implemented using well established neural components, as we will now describe.

We have recently provided psychophysical evidence for global, concentric summation of activity in response to Glass patterns produced by rotation (producing the percept of circular organization) [13]. These results can be explained by a model of receptive fields structured to pool local oriented contour segments concentrically. More specifically, we have suggested that the rectified outputs of V1 simple cells are filtered by orthogonal second stage filters, which have properties of endstopped complex cells. Such cells have been shown to encode local contour curvature [32–34]. A final stage pools the output of such filters organized concentrically around the receptive field center (see Fig. 4 of [13]. This last stage may occur in area V4 on the basis of the descriptions of non-Cartesian receptive fields in this region [16,17].

Responses of these 'concentric units' to radial frequency patterns have been computed with the results depicted in Fig. 13. Over a range of RF pattern sizes, the maximally responding unit was always located at the center of the pattern (marked by + in the simulations). Thus, responses of these model units provide a center of coordinates for the analysis of RF shapes. On the assumption that V4 concentric units form an hexagonal array, we have examined the responses of the 12 units located in the second ring of the array (i.e. second nearest neighbors of the maximally stimulated unit). The locations of these units are marked by white dots in Fig. 13, and their responses to RF2 and RF3 patterns are plotted in the lower portion of the figure. It is clear that responses of this array of 12 concentric units can produce a distributed code for the shape of these RF patterns. Furthermore, a ring of 12 units in a

hexagonal array is limited to accurate representation of radial frequencies of six or less because of the Nyquist theorem. This provides a plausible explanation for the observed limitations on RF pattern recognition. Further work will be necessary to evaluate the quantitative predictions of this model in detail, but it does provide a useful qualitative explanation of our data.

Electrophysiological evidence in support of 'concentric units' comes from the work of Gallant et al. [16,17]. In an extensive investigation of primate cortical area V4, these investigators found that the Cartesian grating patterns which are such excellent stimuli for neurons earlier in the visual pathway are generally not optimal in V4. Instead, polar (i.e. concentric circles), spiral, and hyperbolic gratings were preferred by the majority of neurons studied, with the polar stimulus being optimal for the greatest number of cells. Some of the V4 neurons in studies by Kobatake and Tanaka [37] have optimal stimuli as determined by their subtraction of parts methodology which are also quasi-circular. In the fovea V4 receptive fields average about 3.0° diameter and extend 1.0–2.0° into the ipsilateral visual field [38]. Such dimensions would be appropriate for global processing of RF patterns near the fovea. Although V4 was originally identified primarily as a 'colour' area [39], recent lesion studies have also confirmed the role of this area in form discrimination [40–42], and in fact form discrimination deficits are considerably more severe than color deficits in V4 lesioned primates.

If neural connectivity in V4 provides a basis for global pooling of contour signals, it is obvious that organizations other than concentric pooling must also exist. Indeed, several recent psychophysical studies have provided evidence for other forms of global processing. For example, Li and Westheimer [43] have shown that orientation discrimination for both crosses and ellipses must involve global processing. In a further study using Glass patterns, we have also found evidence for pooling of information radially [14]. This suggests a picture of V4 as containing a range of concentric, X-shaped, and other global processing configurations that together may provide the building blocks from which the complex responses of inferior-temporal neurons are constructed. Electrophysiological studies are consistent with this view [17,37].

Other models of global shape analysis might be proposed to account for our data. Based on Blum's 'grassfire' analysis of shapes [44,45], for example, Burbeck and Pizer [46] and Kovács and Julesz [47,48] have proposed a medial-axis type of model in which activation initiated at the object boundary spreads inward until it collides with activation from other regions of the boundary. The collision contour then provides a skeleton shape description of the object. Given the hyperacuity thresholds obtained in our study, the 'skeleton' produced by our RF patterns at threshold would consist of only minute variations in the shape of a point, which is the medial-axis transformation of a circle. It has yet to be demonstrated how such variations might be detected. Furthermore, the Burbeck and Pizer [46] model predicts that there will be an optimal spatial frequency for the encoding of each stimulus size, and our data on size-scaling contradicts this prediction.

A series of studies by Polat and colleagues [49–51] has illustrated facilitation between contour segments of identical or similar orientation ('collinear facilitation'), suggesting a mechanism for encoding contour continuity at an early stage in visual processing. Work by Field et al. [52] points in a similar direction. Such low-level processes would increase the salience of smoothly curved contours, thereby facilitating shape analysis by the higher level mechanisms we have proposed above. However, there is no obvious way in which collinear facilitation by itself can account for either hyperacuity thresholds or recognition of RF patterns. Otherwise stated, collinear facilitation may be viewed as a valuable mechanism for increasing the salience of curved object boundaries, but further global processing remains necessary for object discrimination and recognition.

The stimuli used in this study were each defined by a single radial frequency and thus comprise the simplest subset of a very general class of patterns. Fourier analysis demonstrates that sums of radial frequency patterns can represent any smooth closed shape that is single valued in polar coordinates. (The radius of such a pattern is simply described as a Fourier series on the interval $-\pi$ to π.). The class of shapes which can be represented by radial frequency patterns thus includes many natural forms such as fruits, vegetables, flowers, and human and animal heads and torsos. This observation plus the accuracy of recognition and global processing of radial frequency patterns recommend them as a useful stimulus class for studying global pooling at intermediate levels of form vision both psychophysically and physiologically.

Acknowledgements

This research was supported in part by NSERC grant # OGP0007551 to F. Wilkinson, NIH grant # EY02158 to H.R. Wilson, and a Research to Prevent Blindness grant to The University of Chicago.

References

[1] DeValois RL, DeValois KK. Spatial Vision. New York: Oxford University Press, 1988.
[2] Graham N. Visual Pattern Analyzers. New York: Oxford University Press, 1989.

[3] Wilson HR. Psychophysical models of spatial vision and hyperacuity. In: Regan D, editor. Spatial Vision. London: MacMillan, 1991:64–86.
[4] Ungerleider LG, Mishkin M. Two cortical visual systems. In: Ingle DJ, Goodale MJ, Mansfield RJW, editors. Analysis of Visual Behavior. Cambridge, MA: MIT Press, 1982:549–86.
[5] Desimone R. Face selective cells in the temporal cortex of monkeys. J Cog Neurosci 1991;3:1–8.
[6] Gross CG. Representation of visual stimuli in inferior temporal cortex. Philos Trans R Soc Lond 1992;335:3–10.
[7] Tanaka K. Inferotemporal cortex and object vision. Ann Rev Neurosci 1996;19:109–39.
[8] Bergen JR, Landy MS. Computational modeling of visual texture segregation. In: Landy M, Movshon JA, editors. Computational Models of Visual Processing. Cambridge, MA: MIT Press, 1991:253–71.
[9] Fogel I, Sagi D. Gabor filters as texture discriminators. Biol Cybern 1989;61:103–13.
[10] Graham N. Complex channels, early local nonlinearities, and normalization in texture segregation. In: Landy M, Movshon JA, editors. Computational Models of Visual Processing. Cambridge MA: MIT Press, 1991:273–90.
[11] Malik J, Perona P. Preattentive texture discrimination with early vision mechanisms. J Opt Soc Am A 1990;7:923–32.
[12] Wilson HR, Richards WA. Curvature and separation discrimination at texture boundaries. J Opt Soc Am A 1992;9:1653–62.
[13] Wilson HR, Wilkinson F, Asaad W. Concentric orientation summation in human form vision. Vis Res 1997;37:2325–30.
[14] Wilson HR, Wilkinson F. Detection of global structure in Glass patterns: implications for form vision. Vis Res 1998;38:2933–47.
[15] Biederman I. Rocognition-by-components: a theory of human image understanding. Psychol Rev 1987;94:115–47.
[16] Gallant JL, Braun J, Van Essen DC. Selectivity for polar, hyperbolic, and Cartesian gratings in macaque visual cortex. Science 1993;259:100–3.
[17] Gallant JL, Connor CE, Rakshit S, Lewis JW, Van Essen DC. Neural responses to polar, hyperbolic, and Cartesian gratings in area V4 of the macaque monkey. J Neurophysiol 1996;76:2718–39.
[18] Glass L. Moiré effect from random dots. Nature 1969;223:578–80.
[19] Schwartz EL, Desimone RL, Albright TD, Gross CG. Shape recognition and inferior temporal neurons. Proc Natl Acad Sci USA 1983;80:5776–8.
[20] Westheimer G. The spatial sense of the eye. Invest Ophthalmol Vis Sci 1979;18:893–912.
[21] Tyler CW. Periodic vernier acuity. J Physiol 1973;228:637–47.
[22] Laursen AM, Rasmussen JB. Circle-ellipse discrimination in man and monkey. Vis Res 1975;15:173–4.
[23] Regan D, Hamstra SJ. Shape discrimination and the judgment of perfect symmetry: dissociation of shape from size. Vis Res 1992;32:1845–64.
[24] Shepard RN, Cermak GW. Perceptual-cognitive explorations of a toroidal set of free-form stimuli. Cogn Psychol 1973;4:351–77.
[25] Kaufman EL, Lord MW, Reese TW, Volkmann J. The discrimination of visual number. Am J Psychol 1949;62:498–525.
[26] Jevons WS. The power of numerical discrimination. Nature 1871;3:281–2.
[27] Woodworth RS, Schlosberg H. Experimental Psychology. New York: Holt Rinehart and Winston, 1954.
[28] Miller GA. The magical number seven, plus or minus two: some limits on our capacity for processing information. Psychol Rev 1956;63:81–97.
[29] Wilson HR. Discrimination of contour curvature: data and theory. J Opt Soc Am A 1985;2:1191–9.
[30] Wilson HR, Richards WA. Mechanisms of contour curvature discrimination. J Opt Soc Am A 1989;7:106–15.
[31] Watt RJ, Andrews DP. Contour curvature analysis: hyperacuities in the discrimination of detailed shape. Vis Res 1982;22:449–60.
[32] Dobbins A, Zucker SW, Cynader MS. Endstopped neurons in the visual cortex as a substrate for calculating curvature. Nature 1987;329:438–41.
[33] Dobbins A, Zucker SW, Cynader MS. Endstopping and curvature. Vis Res 1989;29:1371–87.
[34] Koenderink JJ, Richards W. Two-dimensional curvature operators. J Opt Soc Am A 1988;5:1136–41.
[35] Kimia BB, Tannenbaum AR, Zucker SW. Shapes, shocks, and deformations I: the components of two–dimensional shape and the reaction- diffusion space. Int J Comput Vis 1995;15:189–224.
[36] Zahn CT, Roskies RZ. Fourier descriptors for plane closed curves. IEEE Trans Comput 1972;21:269–81.
[37] Kobatake E, Tanaka K. Neuronal selectivities to complex object features in the ventral visual pathway of the macaque cerebral cortex. J Neurophysiol 1994;71:856–67.
[38] Boussaoud D, Desimone R, Ungerleider LG. Visual topography of area TEO in the macaque. J Comp Neurol 1991;306:554–75.
[39] Zeki SM. Colour coding in the cerebral cortex: the reaction of cells in monkey visual cortex to wavelengths and colours. Neuroscience 1983;9:741–65.
[40] Heywood CA, Cowey A. On the role of cortical area V4 in the discrimination of hue and pattern in macaque monkey. J Neurosci 1987;7:2601–17.
[41] Heywood CA, Gadotti A, Cowey A. Cortical area V4 and its role in the perception of color. J Neurosci 1992;12:4056–65.
[42] Schiller PH. Effects of lesions in visual cortical area V4 on the recognition of transformed objects. Nature 1995;376:342–4.
[43] Li W, Westheimer G. Human discrimination of the implicit orientation of simple symmetrical patterns. Vis Res 1997;37:565–72.
[44] Blum H. A new model of global brain function. Perspect Biol Med 1967;10:381–407.
[45] Blum H. Biological shape and visual science. J Theoret Biol 1973;38:205–87.
[46] Burbeck CA, Pizer SM. Object representation by cores: Identifying and representing primitive spatial regions. Vis Res 1995;35:1917–30.
[47] Kovács I. Gestalten of today: early processing of visual contours and surfaces. Behav Brain Res 1996;82:1–11.
[48] Kovács I, Julesz B. Perceptual sensitivity maps within globally defined visual shapes. Nature 1994;370:644–6.
[49] Polat U, Norcia AM. Neurophysiological evidence for contrast dependent long-range facilitation and suppression in the visual cortex. Vis Res 1996;36:2099–109.
[50] Polat U, Sagi D. Lateral interactions between spatial channels: suppression and facilitation revealed by lateral masking experiments. Vis Res 1993;33:993–9.
[51] Polat U, Sagi D. The architecture of perceptual spatial interactions. Vis Res 1994;34:73–8.
[52] Field DJ, Hayes A, Hess RF. Contour integration by the human visual system: evidence for a local 'association field'. Vis Res 1993;33:173–93.